Published in final edited form as:
Traffic. 2012 August ; 13(8): 1160–1169. doi:10.1111/j.1600-0854.2012.01375.x.

The BLOS1 interacting protein KXD1 is involved in the biogenesis of lysosome-related organelles

Qing Yang[1,5], **Xin He**[1,*], **Lin Yang**[1], **Zhiyong Zhou**[1], **Andrew R. Cullinane**[2], **Aihua Wei**[3], **Zhe Zhang**[1,5], **Zhenhua Hao**[1,5], **Aili Zhang**[1,5], **Min He**[1], **Yaqin Feng**[1], **Xiang Gao**[4], **William A. Gahl**[2], **Marjan Huizing**[2], and **Wei Li**[1,*]

[1]State Key Laboratory of Molecular and Developmental Biology, Institute of Genetics & Developmental Biology, Chinese Academy of Sciences, Beijing 100101, China

[2]Medical Genetics Branch, National Human Genome Research Institute, National Institutes of Health, Bethesda, MD 20892, USA

[3]Department of Dermatology, Beijing Tongren Hospital, Capital Medical University, Beijing 100730, China

[4]MOE Key Laboratory of Model Animal for Disease Study, Model Animal Research Center, Nanjing University, Nanjing, Jiangsu 210061, China

[5]Graduate School of Chinese Academy of Sciences, Beijing 100039, China

Abstract

Biogenesis of lysosome-related organelles complex-1 (BLOC-1) is an eight-subunit complex involved in lysosomal trafficking. Interacting proteins of these subunits expand the understanding of its biological functions. With the implementation of the naïve Bayesian analysis, we found that a human uncharacterized 20 kDa coiled-coil KxDL protein, KXD1, is a BLOS1-interacting protein. *In vitro* binding assays confirmed the interaction between BLOS1 and KXD1. Mouse KXD1 homolog was widely expressed and absent in *Kxd1* knockout (KO) mice. BLOS1 was apparently reduced in *Kxd1*-KO mice. Mild defects in the melanosomes of the retinal pigment epithelia and in the platelet dense granules of the *Kxd1*-KO mouse were observed, mimicking a mouse model of mild Hermansky-Pudlak syndrome that affects the biogenesis of lysosome-related organelles.

Keywords

BLOC-1; KXD1; BLOS1; lysosome-related organelles; Hermansky-Pudlak syndrome

INTRODUCTION

Lysosome-related organelles (LROs) are a family of specialized cell type-specific compartments such as melanosomes in melanocytes, platelet dense granules that share the biogenesis machinery with conventional lysosomes (1, 2). The LROs receive their components from the sorting endosomes through vesicular trafficking. They may co-exist with conventional lysosomes in some types of mammalian cells (3), so that sorting

*Correspondence should be addressed to Dr. Wei Li or Dr. Xin He, Institute of Genetics & Developmental Biology, Chinese Academy of Sciences, #1–2 West Beichen Road, Chaoyang District, Beijing 100101, China. Tel/FAX: +86-10-64806568, wli@genetics.ac.cn or xhe@genetics.ac.cn..

mechanisms have to ensure proper transport of LRO components, different from that of conventional lysosomes.

HPS is a genetically heterogeneous disorder due to defects in LROs and characterized by oculocutaneous albinism, prolonged bleeding and granulomatous colitis or pulmonary fibrosis in some cases (4–6). In humans and mice, HPS results from mutations in any of at least nine genes, *HPS1, AP3B1, and HPS3* to *HPS9,* which encode the components of adaptor complexes and biogenesis of lysosome-related organelles complexes (4–7). Likewise, mutations in the homologous genes in *Drosophila melanogaster* and *Caenorhabditis elegans* result in defective formation of eye pigment granules or gut granules, respectively (8, 9).

The HPS genes encoding subunits of the AP-3 complex and HOPS complex are well-defined in vesicle trafficking (6, 10). However, most of the identified HPS genes are functionally unclear. These HPS proteins lack common structural motifs or significant homology to proteins of defined function. Biochemical analyses reveals that these proteins are subunits of three distinct complexes, named biogenesis of lysosome-related organelles complex (BLOC)-1, -2, and -3 (7, 11–15).

BLOC-1 is a ubiquitously expressed multi-subunit protein complex involved in the biogenesis of specialized organelles via the endosomal-lysosomal system. This complex contains at least eight coiled-coil forming proteins, i.e., pallidin, muted, dysbindin, cappuccino, snapin, BLOS1, BLOS2, and BLOS3 (11, 16–18). Mutations in three BLOC-1 subunits, dysbindin, BLOS3 and pallidin, are responsible for subtypes HPS-7, HPS-8 and HPS-9, respectively (16, 19, 20). The functions and behaviors of BLOC-1 remain to be defined. Currently, it is unknown whether BLOC-1 functions as a vesicle coat or a shuttling adapter between cargo-loaded vesicles and targeted organelles. BLOC-1 has been suggested to function in cargo transport from endosomes to lysosomes (21–23). In BLOC-1-deficient cells, surface proteins accumulate when lysosomal degradation is altered (21, 24–26). The native molecular mass of the mouse BLOC-1 complex was previously calculated to be ~230 kDa (16, 18). However, if the complex contains one copy of each of the eight known subunits (27), the theoretic calculated molecular mass would be ~170 kDa. Therefore, it is possible that BLOC-1 contains additional unidentified subunits.

In this study we identified a protein of unknown function, KXD1 or C19orf50, which interacts with BLOS1 by *in vitro* binding assays. Phenotypic analyses in *Kxd1* knockout mice suggest it is involved in the biogenesis of lysosome-related organelles.

RESULTS

Predicted interactome of BLOC-1 by the naïve Bayesian analysis

Implemented by the naïve Bayesian analysis, we inferred the interaction between human BLOS1 and C19orf50 from the homologous protein-protein interaction pair in *Drosophila,* CG30077 and CG10681, based on the large screen of PPIs by yeast-two hybrid assays (CuraGen *Drosophila* interaction database (http://www.droidb.org/) (Fig. 1A). The database lists C19orf50, or KXD1, as an uncharacterized conserved KxDL protein with unknown function, encoded by the KxDL motif containing gene 1 (*KXD1*). This KxDL motif containing protein family contains proteins which are conserved over a region of 80 residues with a characteristic KxDL motif towards the C-terminus.

By sequence comparison, we found that a transcript in mouse (2810422J05Rik-001, Ensemb accession No., ENSMUST00000093456; GenBank accession No., BC048938) encodes a predicted protein (KXD1a, 177 aa, 20 kDa) with 93% identity to human KXD1 (NCBI

accession No., NP_076974) (Fig. 1B). Another mouse transcript variant (2810422J05Rik-006, Ensembl accession No., ENSMUST00000118850) differs from KXD1a in the first exon, encoding a predicted 219 aa protein (KXD1b) with a molecular weight of 24.6 kDa due to the addition of 42 aa at the N-terminus of KXD1a. Both transcripts have been verified by sequencing the mouse RT-PCR amplicons encoding the two full-length transcripts (data not shown). However, our purified antibody to KXD1a did not recognize KXD1b in tissue blots (data not shown), suggesting that KXD1b may not play a physiological role. Thus, we will use KXD1a to represent the mouse KXD1 homolog, encoded by the *Kxd1* gene, in the following studies. Mouse KXD1 has no transmembrane domain, but contains an uncharacterized conserved KxDL domain from residues 12 to 99, where the KxDL motif is located at residues 74 to 77. It is predicted to contain two consecutive coiled-coils with lower probabilities within the region from residues 20 to 100 by the COILS program (Fig. 1C). In yeast, a KXD1 homolog (KXD1p/YGL079Wp) is suggestive of a BLOC-1 interactor (28).

Interaction between KXD1 and BLOS1

Yeast two-hybrid analyses were applied to verify the prediction of an interaction between mouse KXD1 and BLOS1. We also detected the binary interactions between KXD1 and the other seven known BLOC-1 subunits. As autoactivations were found in dysbindin and muted, we did not test the interactions between the dysbindin or muted bait (binding domain) and the KXD1 prey (activation domain). KXD1 was found to interact with four BLOC-1 subunits, BLOS1, BLOS2, cappuccino and dysbindin (Fig. 2A, 2B). We next confirmed the interaction between KXD1 and BLOS1 by GST-pulldown and co-immunoprecipitation assays. Both KXD1 and BLOS1 pulled down each other (Fig. 2C) and coprecipitated with each other (Fig. 2D).

In addition, dysbindin is the largest known subunit of BLOC-1. We here determined that the interacting domain of dysbindin to KXD1 was its coiled-coil C1 region (peptide 90–140 of dysbindin) (Suppl. Fig. 1), where it interacts with pallidin (29) and snapin (30). The interaction between dysbindin and KXD1 was further verified by GST-pulldown and co-immunoprecipitation assays (data not shown). In our size-exclusion chromatography and sedimentation velocity assays, we found that KXD1 cosedimented and co-fractionated with dysbindin, muted and snapin (Suppl. Fig. 2). The co-residence of dysbindin and snapin in this study agrees with a previous study (18). These results further support that KXD1 is associated with dysbindin. Due to the unavailability of antibodies or constructs, we did not test other interactions by biochemical assays between KXD1 and CNO or BLOS2 revealed by the yeast-two hybrid assays (Fig. 2A). Taken together, our results revealed that KXD1 interacted with BLOS1 and was associated with several other BLOC-1 subunits, which confirmed the prediction in yeast that KXD1 is a BLOC-1 interactor (28).

Defects of melanosomes and platelet dense granules in *Kxd1*$^{-/-}$ knockout mouse

To study the function of KXD1 *in vivo*, we designed a gene targeting scheme to replace exon 5 of mouse *Kxd1* gene (Fig. 3A). We confirmed the replacement of exon 5 at the genomic level (Fig. 3B) and the loss of KXD1 protein in multiple tissues of *Kxd1*$^{-/-}$ mice we tested, while KXD1 was widely expressed in wild-type mouse (Fig. 3C).

Inferred from the interactions with multiple BLOC-1 subunits, we investigate whether the biogenesis of lysosome-related organelles are affected as reported in several BLOC-1 mouse mutants (7). We examined the morphology of the melanosomes in the retinal pigment epithelium and choroid, and the platelet dense granules in whole-mount platelets of the *Kxd1*$^{-/-}$ knockout mice using their littermates (wild-type (WT) *Kxd1*$^{+/+}$) as controls. Our results did not show drastic defects or loss of these organelles (Fig. 4A, 5A) as seen in other

BLOC-1 mutants such as *Dtnbp1*^{sdy}, *Muted*^{mu}, *Pldn*^{pa}, *Cno*^{cno} and *Bloc1s3*^{rp} (7, 16, 17, 31, 32), excluding *Kxd1*-KO mouse as a typical HPS mouse model (7).

However, the numbers of melanosomes in the retinal pigment epithelium and choroid of the *Kxd1*$^{-/-}$ mutant were slightly increased but they were more rounded in shape and smaller (Fig. 4A). We expect that these changes might affect the melanin biosynthesis in the eye melanocytes. Considering the mixed genetic background (129/J and C57BL/6J) of the *Kxd1*$^{-/-}$ mutant, we measured the eumelanin content in the eye of the *Kxd1*$^{-/-}$ mutant by using C57BL/6J and 129/J as controls. We did not observe significant reduction in the eye eumelanin content between 129/J agouti mice and non-agouti C57BL/6J mice (Fig. 4C). We chose *Kxd1*-KO mice with agouti appearance close to 129/J in this experiment (Fig. 4B). We found that the eumelanin content was significantly decreased in the eyes of the *Kxd1*$^{-/-}$ mutants compared with the 129/J mice (Fig. 4C). Our data suggest that the eumelanin synthesis in melanosomes may be impaired when the effect of mixed genetic background of *Kxd1*-KO mice is considered.

Although platelet dense granules were present in the *Kxd1*$^{-/-}$ mutant, the number of these granules was significantly reduced (Fig. 5) without affecting the total platelet counting (data not shown). The total number of dense granules per platelet in wild-type mouse (average about 10) agrees with the number seen in C57BL/6J or DBA/2J inbred strains (7, 34). Whether this reduction will affect the bleeding time or serotonin secretion in the *Kxd1*$^{-/-}$ mutant requires further investigation. This provides a unique mouse model to explore the underlying mechanism of the biogenesis of dense granules or storage pool deficiency by comparative organellar proteomics, since other HPS mutants have null platelet dense granules (33). Taken together, loss of KXD1 mildly affected the biogenesis of lysosome-related organelles, mimicking the mild form of Hermansky-Pudlak syndrome in humans.

BLOS1 is reduced in *Kxd1*$^{-/-}$ knockout mouse

To understand how the LROs are affected in *Kxd1*-KO mice, we suspect that the loss of KXD1 may destabilize the steady-state levels of BLOC-1 subunits as KXD1 interacts with several subunits of BLOC-1. As in a previous study (16), we checked the steady-state levels of BLOC-1 subunits with available antibodies in kidney extracts. We observed the apparent reduction of BLOS1 in *Kxd1*$^{-/-}$ mutant mice, while no apparent changes in dysbindin and snapin, but an increase in muted (Fig. 6A). Likewise, we found a reduction of KXD1 in BLOS1-siRNA knock down Hela cells (Fig. 6B). However, we did not observe apparent changes in the steady-state levels of KXD1 in other BLOC-1 mutants, such as *sandy, muted* and *pallid* (Fig. 6A). Hence, loss of KXD1 may not lead to the typical HPS phenotypes of *sandy, muted* and *pallid* mutants as the loss of dysbindin, muted, and pallidin typically destabilizes the other BLOC-1 subunits (16). The destabilization of BLOS1 in *Kxd1*-KO mice may be the underlying mechanism of affected LROs, suggesting the interaction between KXD1 and BLOS1 may be involved in the biogenesis of LROs.

Mutational screening of human *KXD1* in HPS or albinism patients

In human, nine genes have been characterized as the causative genes of HPS. HPS-7, HPS-8 and HPS-9 are BLOC-1 defects. Oculocutaneous albinism (OCA) is one of the typical phenotypes of HPS and we have identified four HPS-1 patients during our molecular screening in 179 Chinese OCA patients (34). We reasoned that mutation of the *KXD1* gene might produce a subtype of HPS or OCA as the LROs in the *Kxd1*-KO mice were affected. We screened the mutations on human *KXD1* gene in the patients with unidentified mutations of known OCA genes, including 8 HPS, and 19 HPS-like patients from the collection at the National Institutes of Health (USA), and 11 Chinese OCA patients in the

Chinese Albinism Registry (34). No *KXD1* pathological mutation was found in these patients.

DISCUSSION

BLOC-1 functions in the biogenesis of lysosome-related organelles. Loss of the BLOC-1 subunit causes typical murine Hermansky-Pudlak syndrome, illustrated by spontaneous mutations in the genes encoding pallidin (35), muted (32), dysbindin (16), cappuccino (17) and BLOS3 (31). The snapin knock-out mutant has not been characterized as an HPS mouse model, because this mutant dies soon after birth (36). There are no reports of mouse mutants in two other subunits of BLOC-1, i.e., BLOS1 and BLOS2. It is unknown whether loss of any of the BLOC-1 subunits will cause the typical murine HPS. Our biochemical data showed that KXD1 is an interactor of BLOC-1. The *Kxd1* knock-out mutant mouse did not show typical features of murine HPS, but it did show a reduction of the platelet dense granules and malformed melanosomes in retinal pigment epithelia, which may lead to reduced melanin synthesis. This renders the $Kxd1^{-/-}$ mutant the first model of a mild form of HPS in mouse.

In typical murine HPS such as *sandy, muted* and *pallid*, loss of one BLOC-1 subunit leads to the destabilization of several other subunits (Fig. 6A) (16). In the $Kxd1^{-/-}$ mutant, only BLOS1 was reduced, with the steady-state levels of dysbindin and pallidin unaffected. Likewise, the steady-state levels of KXD1 did not change in three BLOC-1 mutants, *sandy, muted* and *pallid* (Fig. 6). Our data indicate that loss of KXD1 may not disrupt the core architecture of BLOC-1 complex, possibly explaining why LROs such as melanosomes and platelet dense granules are mildly affected in the $Kxd1^{-/-}$ mutant. More surprisingly, muted protein was increased in the $Kxd1^{-/-}$ mutant, suggesting that the presence of KXD1 may destabilize muted, or that the absence of KXD1 may increase muted as a rescue-mechanism to compensate its function. BLOC-1 is assembled in a linear manner with one copy of each subunit *in vitro.* Two subcomplexes of BLOC-1 have been suggested. (27). At least, KXD1 affects the steady-state of BLOS1 and muted in our study. Whether the interaction between KXD1 and BLOC-1 subunits is required for the regulation of the assembly of BLOC-1 remains to be defined. More detailed biochemical studies together with the crystal structure of BLOC-1 will provide clear evidence for the assembly of BLOC-1. In addition, other yet to be defined BLOC-1 interactors may also play a role in regulating the assembly of BLOC-1, as suggested by other interactors from the PPI predictions shown in Figure 1A and the literature (28, 37, 38). The identification of novel interactors of BLOC-1 will expand our understanding of its functions.

MATERIALS AND METHODS

Mouse colonies and gene targeting

The *Kxd1* knockout mutant ($Kxd1^{-/-}$) was generated by gene targeting in 129/J-derived ES cells and bred in C57BL/6J at the animal facility of the Institute of Genetics and Developmental Biology (IGDB), Chinese Academy of Sciences. The *sandy, muted* and *pallid* mutant colonies were originally from the Jackson Laboratory and maintained in Dr. Richard Swank's laboratory at Roswell Park Cancer Institute (Buffalo, New York, USA) and now homed at IGDB. All procedures were approved by the Institutional Animal Care and Use Committee of IGDB. To ensure the genotypes of $Kxd1^{-/-}$ and wild-type, we developed a PCR method of genotyping based on the gene targeted region of the *Kxd1* gene.

Study subjects

We recruited 11 unrelated oculocutaneous albinism (OCA) patients from the Chinese Han population by following the criteria for the differentiation of OCA1A, OCA1B and OCA2 as previously described after mutations in *TYR, OCA2, SLC45A2* and *HPS1* were excluded (34, 39). In all the 11 OCA patients, white skin, blue or brown iris and mild to severe nystagmus were observed. We also included 8 typical HPS (based on hypopigmentation and absent platelet dense granules), and 19 HPS-like patients (based on hypopigmentation and other clinical symptoms, with visible platelet dense bodies) from the collection in National Institutes of Health (USA). This study was approved by the Institutional Review Boards of the Bioethics Committee of the Institute of Genetics and Developmental Biology, Chinese Academy of Sciences and of the National Human Genome Research Institute, National Institutes of Health, USA. The study was conducted according to Declaration of Helsinki Principles. Written informed consents were obtained and 8 ml peripheral blood samples were collected from all subjects participating in this study. Mutational screening was conducted by Sanger sequencing the exons and exon/intron boundaries of the human *KXD1* gene.

Bayesian analysis

To filter the false positive protein-protein interaction (PPI) from the large screen by yeast-two hybrid, we developed a novel Bayesian algorithm. We took the CuraGen PPI probabilities from the *Drosophila* interaction database (http://www.droidb.org/) as prior probabilities. We searched the corresponding human homologous genes from NCBI Homolo Gene (http://www.ncbi.nlm.nih.gov/sites/homologene) and calculated the correlation coefficients of tissue expression intensities from BioGPS (http://biogps.gnf.org/) as conditional probabilities. We took the PPIs with higher posterior probabilities than prior probabilities calculated by the Bayesian equation into account for candidate positive PPIs. After these candidate PPIs were filtered by the known PPIs using our PPI Finder program (http://liweilab.genetics.ac.cn/tm/) (40), the candidate novel PPIs were included in the predicted interactome and subject to validation by biochemical assays.

Yeast two-hybrid assay

We followed the protocol described in the user manual of the MATCHMAKER 3 yeast two-hybrid system (Clontech, Mountain View, CA, USA). All constructs used in this study were generated as previously described (30). Yeast cells (AH190) were co-transformed with bait (with binding domain) and prey (with activation domain) vectors, and then plated on SD culture medium lacking leucine and tryptophan at 30°C. Colonies that developed within 3 days were transferred to SD medium modified to lack histidine and adenine. Colonies that were able to grow on this medium were selected as positive interactions. Each experiment was repeated three times.

Antibodies

Polyclonal KXD1 antibody was generated in New Zealand White rabbit against a His-tagged fusion protein corresponding to the mouse full-length *Kxd1* gene (GenBank accession No., BC048938). Affinity purified antibody was produced by using nitrocellulose membrane (NC Membrane, Shanghai, China) with full-length KXD1 antigen. Likewise, polyclonal muted, BLOS1 and dysbindin antibodies were generated in New Zealand White rabbits against His-tagged full-length mouse proteins respectively.

Polyclonal snapin antibody was purchased from SYSY (Goettingen, Germany). Monoclonal anti-GST antibody was purchased from Santa Cruz Biotechnology (Santa Cruz, CA, USA).

Polyclonal anti-Myc antibody, monoclonal anti-Flag, anti-His and anti-β-actin antibodies were purchased from Sigma (Sigma-Aldrich, St. Louis, MO, USA).

Steady-state level of protein by immunoblotting

Tissues from wild-type or mutant mice were homogenized in a lysis buffer containing 50mM Tris-HCl, pH 7.4, 150mM NaCl, 1% Triton X-100, supplemented with proteinase inhibitor cocktail (Sigma). The extracts were centrifuged at 15,000 g for 15 min, and the concentration of the solublized protein was determined with Protein Assay (Bio-Rad, Hercules, CA, USA). For detection of various proteins in tissue homogenates, equal amounts of tissue homogenates were separated in SDS-PAGE gels and immunoblotted by a standard procedure, probed with the indicated antibodies and visualized by ECL+ staining (Amersham Biosciences, Piscataway, NJ, USA). Loading controls were probed with anti-β-actin antibody.

Pulldown assay

Full-length BLOS1 or KXD1 was subcloned into the pGEX-4T-1 (with GST-tag) and the His-fusion vector pET28a. GST or GST fusion vectors were transformed into Rosseta competent cell containing pET28a fusion plasmids respectively. Transformants with two kinds of plasmids were then cultured and enriched in LB medium containing both ampicillin and kanamycin antibiotics. GST fusion proteins were purified by glutathione-sepharose 4B (Amersham Biosciences, Piscataway, NJ, USA). Bound protein was detected by immunoblotting with a polyclonal antibody to His. The same PVDF membrane was probed with anti-GST antibody to confirm comparable loading of GST fusion protein. Immunoblotting tests were conducted as described above.

Co-immunoprecipitation

Flag-tagged pCMV-2B-KXD1 or BLOS1 and Myc-tagged pCMV-3B-BLOS1 or KXD1 were co-transfected into HEK293 cells maintained in DMEM supplemented with 10% fetal bovine serum (Invitrogen, Carlsbad, CA, USA) and cultured for 36 h after transfection. Cells were collected by treatment with trypsin and homogenized in lysis buffer (50mM Tris-HCl, pH 7.4, 150mM NaCl, 0.1% Triton X-100 and protease inhibitor mixture) at 4°C. Lysates were centrifuged at 10,000 g for 15 min at 4°C. Cleared lysates were then incubated with anti-FLAF M2 magnetic beads (Sigma) for 12 h and eluted by Flag peptide (Sigma) according to the manufacture's manual. Eluates were evaluated by immunoblotting with a polyclonal anti-Myc antibody (Sigma). The same blot was probed with anti-Flag antibody (Sigma) to confirm comparable loading of Flag-tagged proteins. Immunoblotting procedures were conducted as described above.

Co-sedimentation and co-fractionation

Aliquots of mouse liver were homogenized in sample buffer (0.3M Tris-HCl, pH 7.5, 1mM EGTA, 1mM dithiothreitol, 0.5mM MgCl2, and protease inhibitor mixture) followed by centrifugation at 5000 g for 5 min and at 120,000 g for 90 min at 4°C (11). The supernatant was fractioned by ultracentrifugation on an MLA-55 rotor (Optima, Beckman, Germany) at 100,000 g on a 5–20% (w/v) sucrose gradient (12 ml) prepared in sample buffer. Total 24 fractions (0.5 ml each) were analyzed by immunoblotting with antibodies to dysbindin, KXD1, muted, snapin and BLOS1.

Mouse liver supernatant (0.2 ml, about 6mg of total protein) was applied to a Superdex 200 column (1×30cm) and eluted with sample buffer at a flow rate of 0.4 ml/min. The size-exclusion chromatograhpy was performed at 4°C in a Fast Protein Liquid Chromatography System (GE Healthcare). Fractions (0.5 ml each) were collected and analyzed by

immunoblotting with antibodies to dysbindin, muted, snapin and KXD1. Immunoblotting procedures were conducted as described above.

Electronic microscopy

Retina—Eye tissues were fixed over night at 4 °C with 3% glutaraldehyde in 0.1 M phosphate buffer, pH7.2. Post-fixation was in 1% osmium tetroxide in 0.1 M phosphate buffer pH7.2, for 1 h. Tissues were dehydrated in serial acetone incubations and embedded in Spurr resin, polymerized at 70°C for 12 hours. Tissues were sectioned to 70 nm with Leica ultramicrotome. Grids were viewed without staining directly on an electron microscope (JEOL, JEM 1400, Japan) at 80 KV and digital images were captured with CCD camera.

Platelets—Mouse blood (0.9 ml) was obtained from heart right ventricle and mixied with 3.8% sodium citrate (0.1 ml). Platelet rich plasma was obtained by centrifugation at 150 g for 10min at room temperature. A drop of platelet rich plasma was put on a carbon coated grid and, 30 sec later, blotted carefully with Whatman 3# filter paper. The grids were viewed without staining on a JEM1400 electron microscope.

Eye eumelanin measurement by HPLC

The quantification of eumelanin was based on the formation of the specific degradation product, pyrrole-2,3,5-tricarboxylic acid (PTCA) by alkaline H_2O_2 oxidation of eumelanin (41). Briefly, whole mouse eye was taken into 2 ml screw-capped test tubes, to which 375 μl 1 mol/l K_2CO_3 and 25 μl volume of 30% H_2O_2 (final concentration: 1.5%) were added. The mixtures were mixed in the room temperature for 20 hrs. The residual H_2O_2 was decomposed by the addition of 50 μl 10% Na_2SO_3 and the mixtures were then acidified with 140 μl 6 mol/l HCl. After vortex-mixing, the reaction mixtures were centrifuged at 4,000 g for 1 min, and aliquots (20 μl) of the supernatant fluids were directly injected into the HPLC system (Waters 1525, Waters Corp., USA) using a Symmetry C18 column (4.6 mm × 250 mm, 5 μm, Waters, Ireland) and a UV detector. The mobile phase was 0.1 mol/l potassium phosphate buffer (pH 1.9) : MeOH, 99 : 1 (v/v). Analyses were performed at 35°C at a flow rate of 0.7 ml/min. Absorbance of the eluent was monitored at 269 nm.

Statistics

For melanin measurements, statistical significance was determined by Student's *t*-test. For platelet dense granule counting results, statistical significance was determined by *Chi-square* test. In the figures, all data represent mean ± s.e.m. * $p<0.05$, ** $p<0.01$.

Supplementary Material

Refer to Web version on PubMed Central for supplementary material.

Acknowledgments

This work was partially supported by grants from National Natural Science Foundation of China (31071252; 81101182; 30730049), Ministry of Agriculture of PRC (2009ZX08009-158B), Chinese Academy of Sciences (KSCX2-EW-R-05), and the Intramural Research Program of the National Human Genome Research Institute, National Institutes of Health, Bethesda, MD, USA. We thank Dr. Xinquan Wang at Tsinghua University for support in the co-fractionation assay, Drs. Shosuke Ito and Kazumasa Wakamatsu for providing the protocol and reagents of melanin analysis, and we are thankful to Dr. Michael Marks at University of Pennsylvania for his critical comments to our manuscript.

REFERENCES

1. Blott EJ, Griffiths GM. Secretory lysosomes. Nat Rev Mol Cell Biol. 2002; 3(2):122–131. [PubMed: 11836514]
2. Dell'Angelica EC, Mullins C, Caplan S, Bonifacino JS. Lysosome-related organelles. FASEB J. 2000; 14(10):1265–1278. [PubMed: 10877819]
3. Marks MS, Seabra MC. The melanosome: membrane dynamics in black and white. Nat Rev Mol Cell Biol. 2001; 2(10):738–748. [PubMed: 11584301]
4. Wei ML. Hermansky-Pudlak syndrome: a disease of protein trafficking and organelle function. Pigment Cell Res. 2006; 19(1):19–42. [PubMed: 16420244]
5. Li W, He M, Zhou H, Bourne JW, Liang P. Mutational data integration in gene-oriented files of the Hermansky-Pudlak Syndrome database. Hum Mutat. 2006; 27(5):402–407. [PubMed: 16550546]
6. Huizing M, Helip-Wooley A, Westbroek W, Gunay-Aygun M, Gahl WA. Disorders of lysosome-related organelle biogenesis: clinical and molecular genetics. Annu Rev Genomics Hum Genet. 2008; 9:359–386. [PubMed: 18544035]
7. Li W, Rusiniak ME, Chintala S, Gautam R, Novak EK, Swank RT. Murine Hermansky-Pudlak syndrome genes: regulators of lysosome-related organelles. Bioessays. 2004; 26(6):616–628. [PubMed: 15170859]
8. Hermann GJ, Schroeder LK, Hieb CA, Kershner AM, Rabbitts BM, Fonarev P, Grant BD, Priess JR. Genetic analysis of lysosomal trafficking in Caenorhabditis elegans. Mol Biol Cell. 2005; 16(7): 3273–3288. [PubMed: 15843430]
9. Falcon-Perez JM, Romero-Calderon R, Brooks ES, Krantz DE, Dell'Angelica EC. The Drosophila pigmentation gene pink (p) encodes a homologue of human Hermansky-Pudlak syndrome 5 (HPS5). Traffic. 2007; 8(2):154–168. [PubMed: 17156100]
10. Bonifacino JS. Insights into the biogenesis of lysosome-related organelles from the study of the Hermansky-Pudlak syndrome. Ann N Y Acad Sci. 2004; 1038:103–114. [PubMed: 15838104]
11. Falcon-Perez JM, Starcevic M, Gautam R, Dell'Angelica EC. BLOC-1, a novel complex containing the pallidin and muted proteins involved in the biogenesis of melanosomes and platelet-dense granules. J Biol Chem. 2002; 277(31):28191–28199. [PubMed: 12019270]
12. Gautam R, Chintala S, Li W, Zhang Q, Tan J, Novak EK, Di Pietro SM, Dell'Angelica EC, Swank RT. The Hermansky-Pudlak syndrome 3 (cocoa) protein is a component of the biogenesis of lysosome-related organelles complex-2 (BLOC-2). J Biol Chem. 2004; 279(13):12935–12942. [PubMed: 14718540]
13. Martina JA, Moriyama K, Bonifacino JS. BLOC-3, a protein complex containing the Hermansky-Pudlak syndrome gene products HPS1 and HPS4. J Biol Chem. 2003; 278(31):29376–29384. [PubMed: 12756248]
14. Nazarian R, Falcon-Perez JM, Dell'Angelica EC. Biogenesis of lysosome-related organelles complex 3 (BLOC-3): a complex containing the Hermansky-Pudlak syndrome (HPS) proteins HPS1 and HPS4. Proc Natl Acad Sci U S A. 2003; 100(15):8770–8775. [PubMed: 12847290]
15. Zhang Q, Zhao B, Li W, Oiso N, Novak EK, Rusiniak ME, Gautam R, Chintala S, O'Brien EP, Zhang Y, Roe BA, Elliott RW, Eicher EM, Liang P, Kratz C, et al. Ru2 and Ru encode mouse orthologs of the genes mutated in human Hermansky-Pudlak syndrome types 5 and 6. Nat Genet. 2003; 33(2):145–153. [PubMed: 12548288]
16. Li W, Zhang Q, Oiso N, Novak EK, Gautam R, O'Brien EP, Tinsley CL, Blake DJ, Spritz RA, Copeland NG, Jenkins NA, Amato D, Roe BA, Starcevic M, Dell'Angelica EC, et al. Hermansky-Pudlak syndrome type 7 (HPS-7) results from mutant dysbindin, a member of the biogenesis of lysosome-related organelles complex 1 (BLOC-1). Nat Genet. 2003; 35(1):84–89. [PubMed: 12923531]
17. Ciciotte SL, Gwynn B, Moriyama K, Huizing M, Gahl WA, Bonifacino JS, Peters LL. Cappuccino, a mouse model of Hermansky-Pudlak syndrome, encodes a novel protein that is part of the pallidin-muted complex (BLOC-1). Blood. 2003; 101(11):4402–4407. [PubMed: 12576321]
18. Starcevic M, Dell'Angelica EC. Identification of snapin and three novel proteins (BLOS1, BLOS2, and BLOS3/reduced pigmentation) as subunits of biogenesis of lysosome-related organelles complex-1 (BLOC-1). J Biol Chem. 2004; 279(27):28393–28401. [PubMed: 15102850]

19. Morgan NV, Pasha S, Johnson CA, Ainsworth JR, Eady RA, Dawood B, McKeown C, Trembath RC, Wilde J, Watson SP, Maher ER. A germline mutation in BLOC1S3/reduced pigmentation causes a novel variant of Hermansky-Pudlak syndrome (HPS8). Am J Hum Genet. 2006; 78(1): 160–166. [PubMed: 16385460]
20. Cullinane AR, Curry JA, Carmona-Rivera C, Summers CG, Ciccone C, Cardillo ND, Dorward H, Hess RA, White JG, Adams D, Huizing M, Gahl WA. A BLOC-1 Mutation Screen Reveals that PLDN Is Mutated in Hermansky-Pudlak Syndrome Type 9. Am J Hum Genet. 2011; 88(6):778–787. [PubMed: 21665000]
21. Setty SR, Tenza D, Truschel ST, Chou E, Sviderskaya EV, Theos AC, Lamoreux ML, Di Pietro SM, Starcevic M, Bennett DC, Dell'Angelica EC, Raposo G, Marks MS. BLOC-1 is required for cargo-specific sorting from vacuolar early endosomes toward lysosome-related organelles. Mol Biol Cell. 2007; 18(3):768–780. [PubMed: 17182842]
22. Cai Q, Lu L, Tian JH, Zhu YB, Qiao H, Sheng ZH. Snapin-regulated late endosomal transport is critical for efficient autophagy-lysosomal function in neurons. Neuron. 2010; 68(1):73–86. [PubMed: 20920792]
23. Salazar G, Craige B, Styers ML, Newell-Litwa KA, Doucette MM, Wainer BH, Falcon-Perez JM, Dell'Angelica EC, Peden AA, Werner E, Faundez V. BLOC-1 complex deficiency alters the targeting of adaptor protein complex-3 cargoes. Mol Biol Cell. 2006; 17(9):4014–4026. [PubMed: 16760431]
24. Cui Y, Li X, Chen Q, He X, Yang Q, Zhang A, Yu X, Chen H, Liu N, Xie Q, Yang W, Zuo J, Palme K, Li W. BLOS1, a putative BLOC-1 subunit, interacts with SNX1 and modulates root growth in Arabidopsis. J Cell Sci. 2010; 123(Pt 21):3727–3733. [PubMed: 20971704]
25. Ji Y, Yang F, Papaleo F, Wang HX, Gao WJ, Weinberger DR, Lu B. Role of dysbindin in dopamine receptor trafficking and cortical GABA function. Proc Natl Acad Sci U S A. 2009; 106(46):19593–19598. [PubMed: 19887632]
26. Tang TT, Yang F, Chen BS, Lu Y, Ji Y, Roche KW, Lu B. Dysbindin regulates hippocampal LTP by controlling NMDA receptor surface expression. Proc Natl Acad Sci U S A. 2009; 106(50): 21395–21400. [PubMed: 19955431]
27. Lee HH, Nemecek D, Schindler C, Smith WJ, Ghirlando R, Steven AC, Bonifacino JS, Hurley JH. Assembly and Architecture of the Biogenesis of Lysosome-Related Organelles Complex-1 (BLOC-1). J Biol Chem. 2012; 287(8):5882–5890. [PubMed: 22203680]
28. Hayes MJ, Bryon K, Satkurunathan J, Levine TP. Yeast homologues of three BLOC-1 subunits highlight KxDL proteins as conserved interactors of BLOC-1. Traffic. 2011; 12(3):260–268. [PubMed: 21159114]
29. Nazarian R, Starcevic M, Spencer MJ, Dell'Angelica EC. Reinvestigation of the dysbindin subunit of BLOC-1 (biogenesis of lysosome-related organelles complex-1) as a dystrobrevin-binding protein. Biochem J. 2006; 395(3):587–598. [PubMed: 16448387]
30. Feng YQ, Zhou ZY, He X, Wang H, Guo XL, Hao CJ, Guo Y, Zhen XC, Li W. Dysbindin deficiency in sandy mice causes reduction of snapin and displays behaviors related to schizophrenia. Schizophr Res. 2008; 106(2–3):218–228. [PubMed: 18774265]
31. Gwynn B, Martina JA, Bonifacino JS, Sviderskaya EV, Lamoreux ML, Bennett DC, Moriyama K, Huizing M, Helip-Wooley A, Gahl WA, Webb LS, Lambert AJ, Peters LL. Reduced pigmentation (rp), a mouse model of Hermansky-Pudlak syndrome, encodes a novel component of the BLOC-1 complex. Blood. 2004; 104(10):3181–3189. [PubMed: 15265785]
32. Zhang Q, Li W, Novak EK, Karim A, Mishra VS, Kingsmore SF, Roe BA, Suzuki T, Swank RT. The gene for the muted (mu) mouse, a model for Hermansky-Pudlak syndrome, defines a novel protein which regulates vesicle trafficking. Hum Mol Genet. 2002; 11(6):697–706. [PubMed: 11912185]
33. Swank RT, Novak EK, McGarry MP, Rusiniak ME, Feng L. Mouse models of Hermansky Pudlak syndrome: a review. Pigment Cell Res. 1998; 11(2):60–80. [PubMed: 9585243]
34. Wei A, Yang X, Lian S, Li W. Implementation of an optimized strategy for genetic testing of the Chinese patients with oculocutaneous albinism. J Dermatol Sci. 2011; 62(2):124–127. [PubMed: 21458243]

35. Huang L, Kuo YM, Gitschier J. The pallid gene encodes a novel, syntaxin 13-interacting protein involved in platelet storage pool deficiency. Nat Genet. 1999; 23(3):329–332. [PubMed: 10610180]

36. Tian JH, Wu ZX, Unzicker M, Lu L, Cai Q, Li C, Schirra C, Matti U, Stevens D, Deng C, Rettig J, Sheng ZH. The role of Snapin in neurosecretion: snapin knock-out mice exhibit impaired calcium-dependent exocytosis of large dense-core vesicles in chromaffin cells. J Neurosci. 2005; 25(45): 10546–10555. [PubMed: 16280592]

37. Rodriguez-Fernandez IA, Dell'Angelica EC. A data-mining approach to rank candidate protein-binding partners-The case of biogenesis of lysosome-related organelles complex-1 (BLOC-1). J Inherit Metab Dis. 2009; 32(2):190–203. [PubMed: 19083121]

38. Gokhale A, Larimore J, Werner E, So L, Moreno-De-Luca A, Lese-Martin C, Lupashin VV, Smith Y, Faundez V. Quantitative proteomic and genetic analyses of the schizophrenia susceptibility factor dysbindin identify novel roles of the biogenesis of lysosome-related organelles complex 1. J Neurosci. 2012; 32(11):3697–3711. [PubMed: 22423091]

39. Wei A, Wang Y, Long Y, Guo X, Zhou Z, Zhu W, Liu J, Bian X, Lian S, Li W. A comprehensive analysis reveals mutational spectra and common alleles in Chinese patients with oculocutaneous albinism. J Invest Dermatol. 2010; 130(3):716–724. [PubMed: 19865097]

40. He M, Wang Y, Li W. PPI finder: a mining tool for human protein-protein interactions. PLoS One. 2009; 4(2):e4554. [PubMed: 19234603]

41. Ito S, Nakanishi Y, Valenzuela RK, Brilliant MH, Kolbe L, Wakamatsu K. Usefulness of alkaline hydrogen peroxide oxidation to analyze eumelanin and pheomelanin in various tissue samples: application to chemical analysis of human hair melanins. Pigment Cell Melanoma Res. 2011; 24(4):605–613. [PubMed: 21535429]

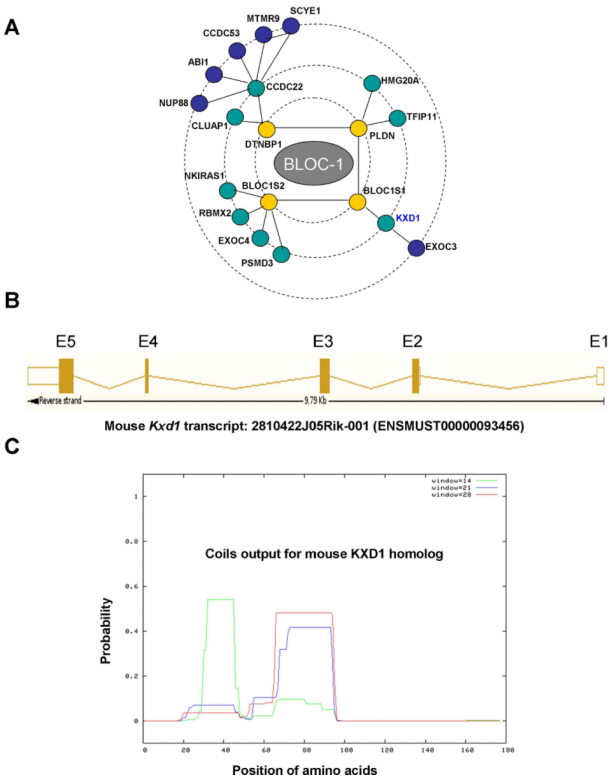

Figure 1. Predicted interaction between BLOS1 and KXD1

(A) The 3-tier predicted interactome of human BLOC-1 using naïve Bayesian analysis. The first tier of this interactome consists of four subunits of BLOC-1 encoded by *DTNBP1, PLDN, BLOC1S1* and *BLOC1S2*. The interaction between the products of *BLOC1S1* and *KXD1* (shown in blue, encodes human KXD1.) is located in the second tier. **(B)** Genomic structure of mouse *Kxd1* gene spanning a 9.79kb region in chromosme 8 in the Ensembl database (http://www.ensembl.org). **(C)** Predicted coiled coils of mouse KXD1 by the COILS program (http://www.ch.embnet.org/software/COILS_form.html). Two coiled coils are shown with lower probabilities.

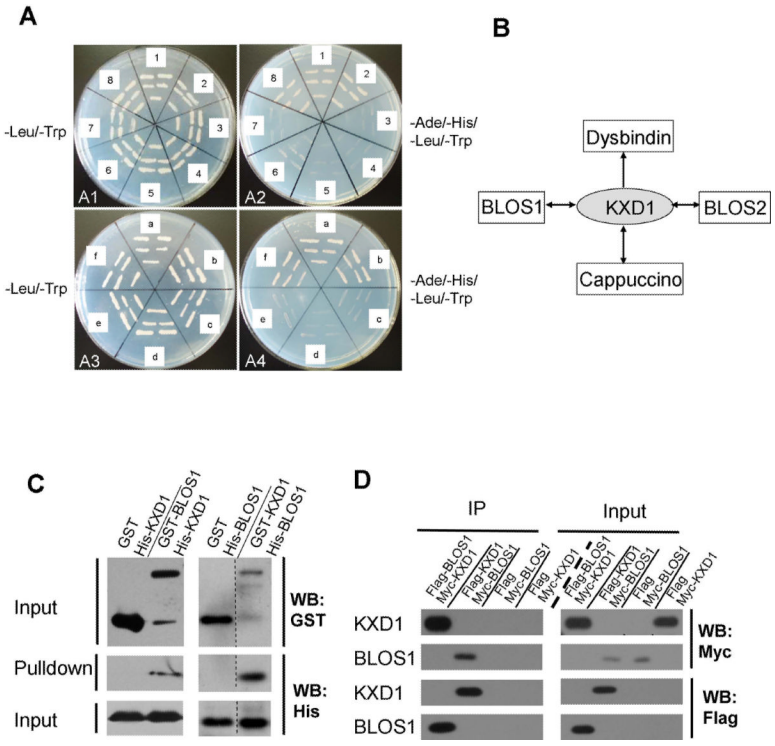

Figure 2. Interactions between KXD1 and other BLOC-1 subunits. (A1, A3)
Yeasts grown on SD medium lacking leucine and tryptophan; **(A2, A4)** Same yeasts grown on SD medium lacking adenine, histidine, leucine and tryptophan. **(A1, A2)** Full-length KXD1 is used as a bait (with binding domain) to test different preys (with activation domain). 1) BLOS1; 2) BLOS2; 3) BLOS3; 4) snapin; 5) pallidin; 6) cappuccino; 7) muted; 8) dysbindin. **(A3, A4)** Full-length KXD1 is used as a prey to test different baits. a) BLOS1; b) BLOS2; c) BLOS3; d) snapin; e) pallidin; f) cappuccino. **(B)** The schematic depiction of KXD1 interactors revealed in (A). Bilateral arrows show bi-directional interactions, while the unilateral arrow between KXD1 and dysbindin shows that KXD1 binds to dysbindin in a unidirectional manner. **(C)** GST-tagged BLOS1 and KXD1 pull down His-tagged KXD1 and BLOS1, respectively, while GST alone added as negative controls do not pull down His-tagged KXD1 or BLOS1. Vertical dotted lines indicate the junction sites of a blot from the same experiment. **(D)** Flag-tagged KXD1 and BLOS1 co-precipitate with Myc-tagged BLOS1 and KXD1, respectively, while Flag empty vectors added as negative controls do not co-precipitate with Myc-tagged BLOS1 or KXD1.

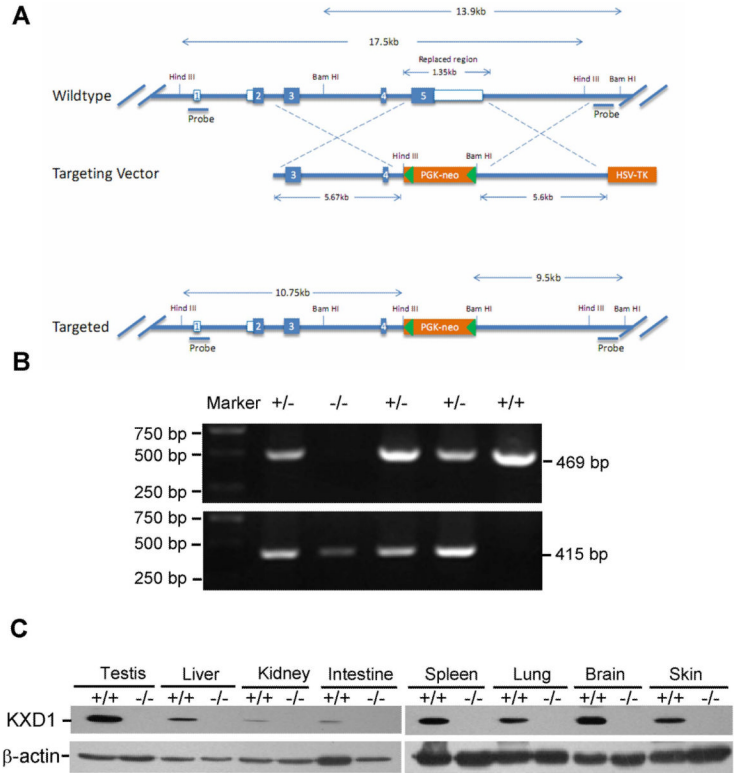

Figure 3. Generation of *Kxd1* kockout mice

(A) Schematic diagram of gene targeting of exon 5 of *Kxd1*. Exon 5 is replaced by PGK-neo cassette from the targeting vector. (**B**) Genomic PCR verification of the deleted exon 5 of *Kxd1*. The wild-type allele gives rise to the PCR amplicon of 469 bp, while the mutational allele gives rise to the 415 bp amplicon. A test of five littermates is shown. (**C**) KXD1 protein is null in multiple tissues of the $Kxd1^{-/-}$ knockout mice compared with wild-type littermates; actin served as a loading control. In this figure, +/+, +/−, −/− denote genotypes of wild-type, heterozygote, and homozygote respectively.

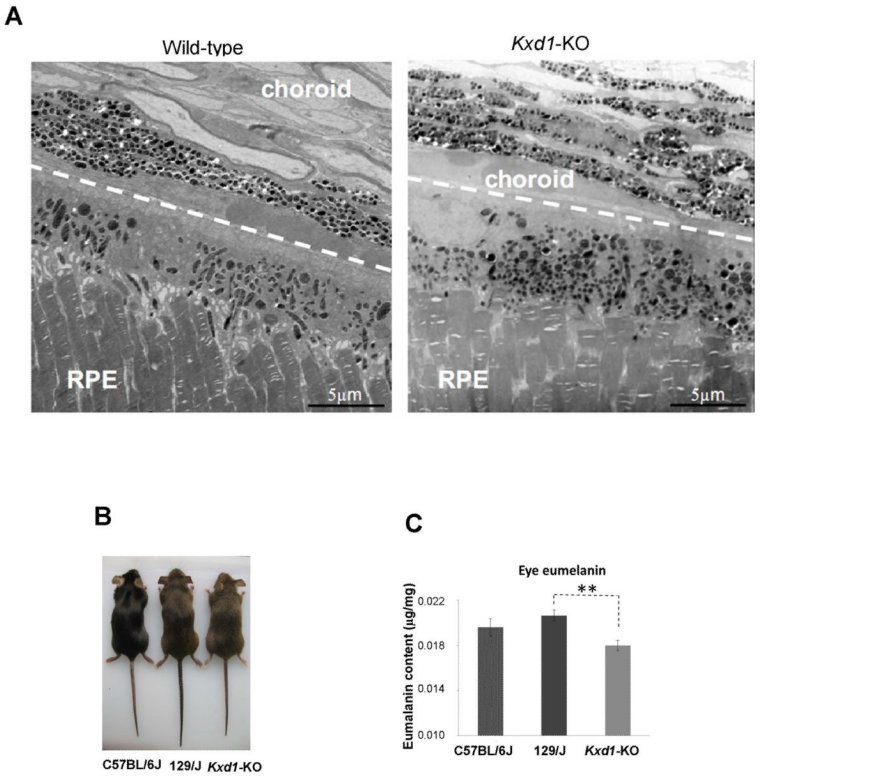

Figure 4. Ultrastructures of melanosomes and eumelanin measurement in mouse eye

(A) Transmission EM pictures of the retina of *Kxd1*$^{-/-}$ mutant and its wild-type littermate (*Kxd*$^{+/+}$). RPE: retina pigment epithelia. Scale bar = 5 μm. **(B)** Mouse pictures of C57BL/6J, 129/J, *Kxd1*$^{-/-}$ mutant (on 129/J background). **(C)** Eumelanin quantification of eye by HPLC. Melanin content is significantly reduced in *Kxd1*$^{-/-}$ mutant (17.99±0.45 ng/mg, n=35) compared to control 129/J mice (20.66±0.48 ng/mg, n=34). The melanin content did not differ significantly between 129/J and C57BL/6J (19.61±0.76 ng/mg, n=36). All data represent mean ± s.e.m. * p<0.05, ** p<0.01.

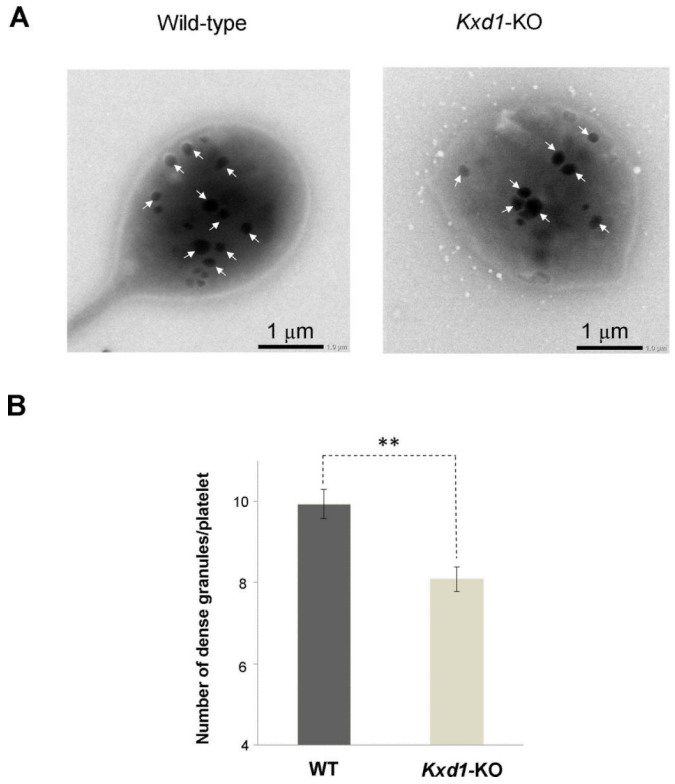

Figure 5. Dense granules are decreased in *Kxd1*-KO mice

(A) Transmission EM pictures of platelets of the *Kxd1*$^{-/-}$ mutant and its wild-type littermate. Arrows show the platelet dense granules. Lighter intensity dots or smaller dots (diameter less than 100 nm) are not counted as dense granules (42). Scale bar = 1 μm. (**B**) Quantification of platelet dense granules. Dense granule number per platelet is significantly reduced in *Kxd1*$^{-/-}$ mutant (8.08±0.31, n=195) compared to wild-type mice (9.93±0.36, n=191). All data represent mean ± s.e.m. ** p<0.01.

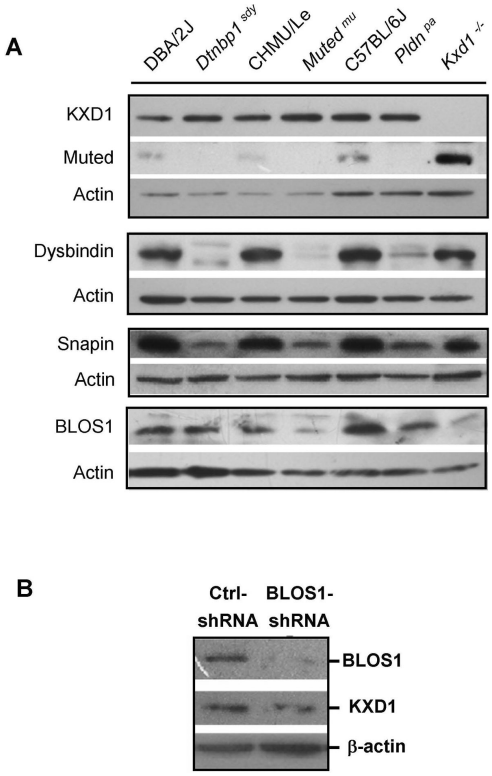

Figure 6. Steady-state levels of BLOC-1 subuints in *Kxd1*-KO mice

(A) Steady-state protein levels in kidney lysates from different mouse mutants and wild-type controls. *Dtnbp1*^{sdy} arose from DBA/2J; *Muted*^{mu} arose from CHMU/Le; *Pldn*^{pa} and *Kxd1*$^{-/-}$ mutant are controlled by C57BL/6J. Note that BLOS1 is reduced in the *Kxd1*$^{-/-}$ mutant mice. These experiments were repeated in three independent assays. **(B)** Mouse *Bloc1s1* siRNA (GGACATGCGCACCATTGCC) and a control scramble siRNA were transfected into the Hela cells for 72h culture. The lysates were collected and western blots were probed with antibodies to BLOS1, KXD1 and actin by immunoblotting.